JOURNAL OF CATALYSIS **165,** 129–139 (1997)
ARTICLE NO. CA971475

Preparation, Characterization, and Activity of Cu/TiO_2 Catalysts

I. Influence of the Preparation Method on the Dispersion of Copper in Cu/TiO_2

F. Boccuzzi,*,[1] A. Chiorino,* G. Martra,* M. Gargano,† N. Ravasio,† and B. Carrozzini‡

*Dipartimento di Chimica I.F.M. dell' Università, Via P. Giuria 7, 10125 Torino, Italy; †Centro C.N.R. MISO, Dipartimento di Chimica dell' Università, Via Amendola 173, 70126 Bari, Italy; and ‡Dipartimento Geomineralogico dell' Università, Via E. Orabona 4, 70126 Bari, Italy

Received December 5, 1995; revised May 25, 1996; accepted September 25, 1996

Different techniques have been used to characterize Cu/TiO_2 (Degussa P-25) catalysts with copper loadings of 2, 4, and 8 wt% Cu, prepared by wet impregnation (labeled I) or by chemisorption–hydrolysis (labeled C). X-ray diffraction patterns of the 8% I sample show, before calcination, the diffraction lines of the monoclinic modification of $Cu_2(OH)_3NO_3$, while after calcination quite large CuO crystallites are observed. In the 8% C sample $Cu_2(OH)_3NO_3$ is not found before calcination and smaller CuO crystallites are observed thereafter. High-resolution transmission electron microscopy indicates a different behavior of the two calcined samples to electron beam exposure: on I samples the electron beam produces an amorphous overlayer, covering in a continuous way the TiO_2 crystallites, whereas on C samples small particles nucleate at the surface of the titania particles. Temperature programmed reduction (TPR) of the C samples shows three narrow peaks in the range 435–470 K, very well resolved in the sample with 4% of copper, while TPR of I samples shows a broad unresolved peak at 440–530 K. The adsorption of CO on the two kinds of reduced samples produces infrared absorption bands in the 2070–2140 cm^{-1} wavenumber range with intensity and position strongly dependent on the preparation method and on the sample pretreatments. On all the I samples, there is a band at 2113–2130 cm^{-1} which is reduced in intensity with increasing the reduction temperature. On the C samples, three well-resolved bands at 2126, 2103, and 2071 cm^{-1} are detected, the last two of which gradually reduce in intensity with decreasing CO pressure. The 2103 cm^{-1} band is assigned to CO adsorption on Cu^0 step and edge sites, the 2071 cm^{-1} band is assigned to CO adsorbed on Cu(111) microfacets and on sites at the edges of small copper particles, and the 2126 cm^{-1} band, observed also on I samples, is assigned to CO adsorption on isolated Cu atoms and/or two-dimensional small Cu clusters on the surface of titania. The 2103 and 2071 cm^{-1} bands are always absent on I samples, indicating that the wet impregnation method leads to samples in which three-dimensional copper particles are almost completely lacking.

[1] To whom correspondence should be addressed. Fax: 3911 6707855. E-mail: Boccuzzi@.ch.unito.it.

1. INTRODUCTION

A simplistic view of the role of the support in supported metal catalysts is that it is an inert carrier of the active component. In this view the support acts simply as a means of separating small metallic particles and mainly influences the metal particle size and their thermal stability. However, over the past few decades it has been observed very often that catalytic performances of the metal catalysts are strongly dependent on the type of carrier, on the preparation method, and on the catalyst activation (1–3). As regards copper catalysts, it is well known that Cu/ZnO catalysts prepared by coprecipitation are very active for methanol synthesis, whereas catalysts prepared by wet impregnation are far less active (4) and the difference cannot be simply justified by differences in the exposed metal surface area. Moreover, it was shown by comparing Cu/ZnO and Cu/TiO_2 samples of similar Cu dispersions (5) that they have very different methanol activities; strong differences have been also observed in the hydrogenation of cyclododecatriene on Cu catalysts supported on different oxides (6).

Various explanations have been put forward to justify the changes observed in the catalytic activity of supported metals, particularly of those supported on reducible oxides, viz., charge transfer between metal and support, decoration of the metal with suboxides of the support, interfacial metal–support interactions, junction effects between the metal and the support, and alloying (1–3). The role and the relative importance of these factors strongly change with the preparation method and with the thermal and chemical pretreatments of the catalysts. In this paper we will present a characterization by XRD, HRTEM, TPR, and FTIR data of Cu/TiO_2 samples with different copper loadings, prepared by wet impregnation or by chemisorption–hydrolysis of P-25 Degussa titania. In the following paper (7) we discuss the differences observed in the hydrogenation of 1,3-cyclooctadiene and in the CO−NO reaction between Cu/TiO_2 samples prepared with the two methods and prereduced at different temperatures.

0021-9517/97 $25.00

2. EXPERIMENTAL

2.1. Materials

The titania utilized in this study as support was a P-25 (Degussa) (80% anatase, 20% rutile, BET surface area 50 m^2/g). The impregnated samples (which will be labeled as I) were prepared by adding an aqueous solution of copper nitrate of suitable concentration and volume (0.5 ml/g) to the support. After the wet impregnation the samples were dried at 393 K for 2 h and finally calcined in air for 16 h at 673 K. The Cu/TiO_2 samples prepared by the chemisorption–hydrolysis method (which will be labeled as C) were prepared by adding the support to a solution containing $[Cu(NH_3)_4]^{2+}$ and slowly diluting the slurry with water, the solution being held in an ice bath, at 273 K, under continuous stirring. The solid was separated by filtration, washed with water, dried overnight at 383 K, and calcined in air at 623 K for 4 h. The copper loading of the samples prepared with the two methods are ≈2, 4, and 8 wt%.

2.2. Methods

X-ray powder diffraction (XRD) patterns were obtained by a Philips PW-1800 automatic diffractometer with Cu$K\alpha$ radiation and NaF as internal standard. The peak of CuO(111) at $2\theta = 35.6^\circ$ was used for line-broadening determinations. Copper oxide crystallite sizes were estimated using the Scherrer equation.

Temperature programmed reductions (TPR) were carried out using a Carlo Erba Fractovap 4000 gas chromatograph, equipped with a thermal conductivity detector (TCD).

The dead volume between the reactor and the TCD was strongly reduced by using short capillary stainless steel tubes and reducing the internal diameter of the outlet arm of the glass reactor. A flow of reducing gas at between 12 and 20 ml(STP)/min and a pressure of 160 kPa was used in all experiments. Under these conditions the partial pressure of H_2 was 8 kPa. A heating rate of 5 K/min was used in all TPR experiments. The rate of hydrogen uptake was measured by a Varian mod. 4290 integrator. We have used an amount of catalyst and flow rate of reducing gas giving a value of the K parameter, introduced by Monti and Baiker (8), ranging between 50 and 160 and a value of the P parameter, introduced by Malet and Caballero (9), between 3 and 13 (see Table 1 for definition of K and P parameters). As recently reported by Fierro and co-workers (10), these experimental conditions can avoid the broadening of TPR profiles and the appearance of peaks which are not due to true reducible species. Moreover, use of a particle size below 400 mm (less than 100 mm in our experiments) allows one to neglect intra- and interparticle mass transfer effects, which have a negative influence on the shape of TPR profiles. A large dead volume can modify and produce artefacts in the TPR profiles (8, 9).

TABLE 1

TPR Operating Variables and Specific Cu(0) Surface Areas for the Six Catalysts Examined

Catalyst	Loading (mg)	S_0 (μmol)	V^* (ml_{STP}/s)	$K = S_0/V^*C_0$ (s)	$P = K\beta$ (K)	$S_{Cu(0)}$[a] (m^2/g_{Cu})
2, 1% C	119	39	0.33	54	4.5	48
4, 3% C	70	47	0.20	107	8.9	64
8, 7% C	57	78	0.22	161	13.4	55
2, 6% I	70	29	0.25	53	4.4	16
4, 6% I	68	49	0.22	101	8.4	11
8, 5% I	67	89	0.25	162	13.5	9

Note. S_0, initial amount of copper; V^*, total flow rate; C_0, initial H_2 concentration in the feed (2, 2 μmol/ml); β, heating rate (5 K/min).

[a] $T_{red} = 373$–473 K.

The Cu(0) surface area was determined by using the N_2O adsorption–decomposition method (11) using a pulse-flow technique. The measurements were carried out on the same gas chromatographic apparatus used for TPR experiments. The Cu(0) surface area was computed by using a surface coverage factor (moles of oxygen atoms per moles of surface Cu(0) atoms) $Q = 0.35$ and a mean surface area for a copper site of 7.41 $Å^2$ (12).

HRTEM measurements were made with a JEOL 2000 EX electron microscope, equipped with a top entry stage. The powder was ultrasonically dispersed in isopropyl alcohol and the suspension was deposited on a copper grid, coated with a porous carbon film. The residual vacuum at the specimen region was approximately 1×10^{-6} mbar.

The IR spectra were recorded at room temperature (RT) in an infrared cell designed to treat the samples *in situ*, using a Perkin–Elmer FTIR 1760 spectrometer, at a resolution of 2 cm^{-1}; the number of scans (100–200) was varied according to the transmission of the sample, with the aim to obtain similar levels of noise.

2.3. Sample Pretreatment

The FTIR experiments were carried out on samples which had been submitted after the preliminary calcination at 673 K to different reduction treatments in H_2; at the end of each treatment the H_2 was evacuated at the same temperature. In the following the differently prepared and pretreated samples will be labeled with a figure indicating the Cu loading of the sample, followed by the letter I for the impregnated samples or by the letter C for the deposited samples, respectively, and by figures corresponding to the temperature of the reduction treatment.

3. RESULTS AND DISCUSSION

3.1. XRD and HRTEM

XRD patterns of the two 8% I and C samples were taken before and after the calcination treatment. Only incipient

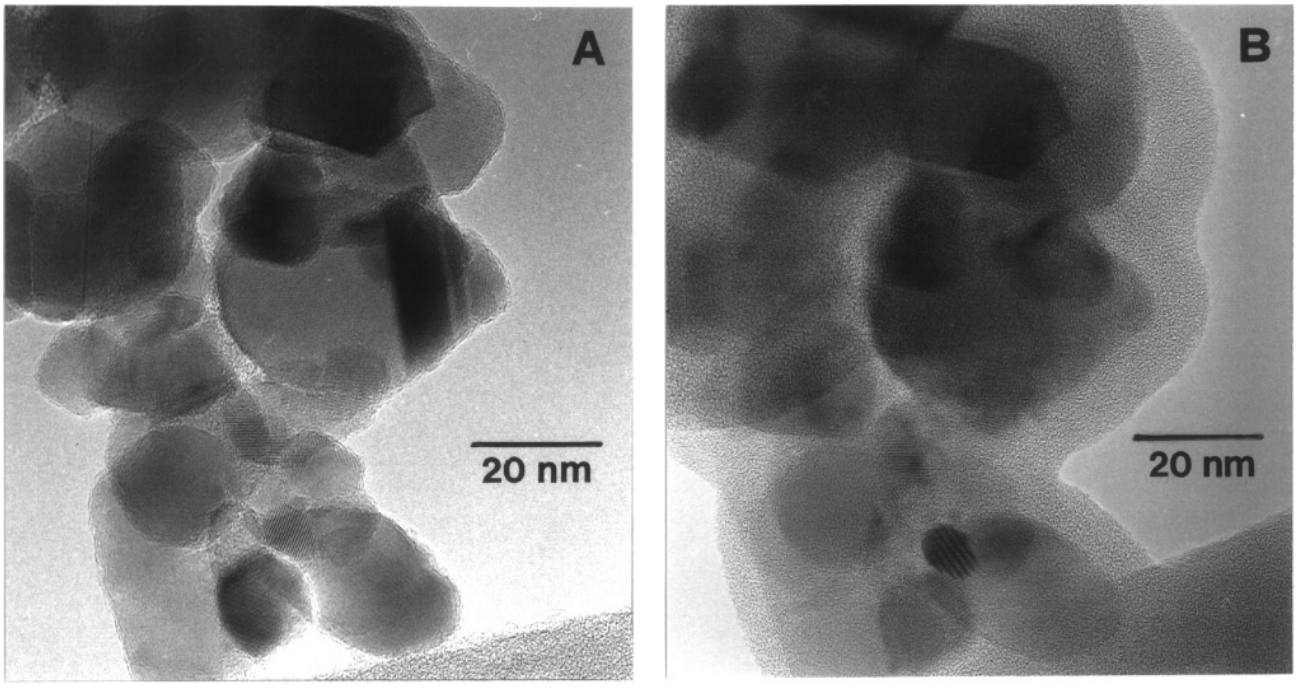

FIG. 1. Electron micrographs of calcined 8I sample (A) taken immediately and (B) after 2 min exposure to the electron beam.

formation of CuO crystallites was observed on the C sample, whereas the presence of gerhardtite, $Cu_2(OH)_3NO_3$, (13) was evident on the 8% I sample before the thermal treatment. It has already been observed that different precursor phases are obtained by changing the preparation method also on other copper-containing catalysts (10). The line broadening leads to an estimated particle size of this phase of 65.5 nm; however, it must be observed that it is unlikely that these dimensions are relating to the whole of the copper-containing phase, as probably also smaller particles are present, below the XRD detectibility limit. After calcination at 623 K CuO crystallites are formed to mean size 44 nm on the I sample, whereas the mean crystallite size of C sample was smaller, $\approx$21 nm. Copper-containing phases are not detected in the samples with lower copper loadings as a consequence of the sensitivity and size limits of XRD technique. In the more widely studied Cu/ZnO samples it was observed that the precursor composition determines the interdispersion and morphology of the calcined catalysts and to some extent also the morphology and the size of the copper particles after the reduction (2, 3). Also in the Cu/TiO_2 samples concerned here the same factors can play a relevant role.

Low-resolution electron micrographs of calcined 8% I and C samples only provide evidence of titania crystallites; there are no visible differences between the two preparations or evidences of other crystalline phases. High-resolution electron micrographs of calcined 8% I and C samples taken immediately and after 2 min of exposure to the electron beam, shown in Figs. 1 and 2, respectively, provide evidence for a different behavior of the two samples under the electron beam. On the I sample the electron beam irradiation produces a quite large, amorphous overlayer, covering in a continuous way the TiO_2 crystallites (Fig. 1B); on the C sample, during the irradiation small particles nucleate at the surface of TiO_2 crystallites (Fig. 2B). The reaction of electron beams with the surfaces of inorganic materials is a complex process which depends on many experimental parameters, such as the chemical nature of the object, the energy and current density of the electrons, and the time of exposure to the electron beam. Reducible metal oxides are usually susceptible to a radiolytic damage mechanism which involves an interatomic Auger decay process and leads to the desorption of oxygen from the surface (14). Both CuO and TiO_2 could in principle be reduced by electron beam exposure. However, it is relevant to note that the same titania was used for the preparation of the two kinds of samples and all the other experimental parameters adopted in the measurements reported in Figs. 1 and 2 were the same. In our opinion, the different behavior of the two samples to the electron beam exposure can be related to the different structure and composition of the copper-containing overlayer: in the C samples copper is deposited at the surface of titania by an ionic exchange reaction, while in the I sample pore filling with the cupric nitrate solution is made. The different features observed in the two cases are to some extent related to the differences detected by XRD in the precursors of the CuO phase in the two samples:

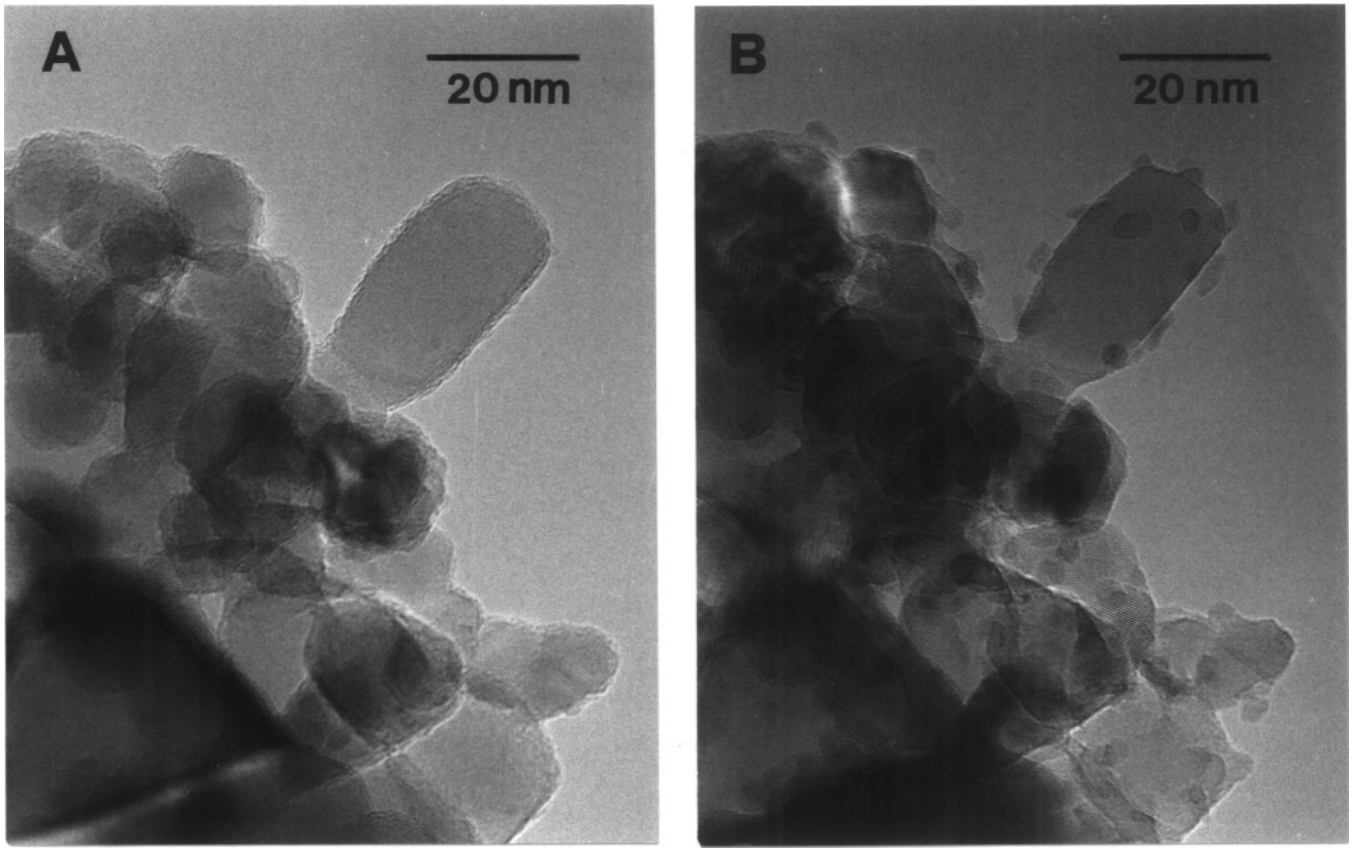

FIG. 2. Electron micrographs of calcined 8C sample (A) taken immediately and (B) after 2 min exposure to the electron beam.

in the I samples a $Cu_2(OH)_3NO_3$ precursor phase is observed, whereas in the C samples CuO is partially formed during the copper-ammine complex hydrolysis and no precursor phases containing NO_3^- ions are detected by XRD. It can be hypothesized that the wet impregnation procedure leads to a copper hydrotitanate surface layer, contamined by some nitrate anions in contact with the $Cu_2(OH)_3NO_3$ phase. This layer, by reduction under the electron beam, leads to an amorphous, disordered overlayer, containing copper and titania interdispersed at atomic level. On sample C the nucleation of well-dispersed particles is probably a consequence of the clean, ionic exchange preparation procedure. In this case the calcination and the reduction under the beam can lead to crystalline, well-dispersed copper particles.

The differences observed between the I and C catalysts can be due to the different pH of the solutions used in the preparation. The pH of the impregnating solution used in the I samples, 3–4, is below the zero charge point for TiO_2 ($\approx$6), and therefore the surface will be positively charged and will adsorb anionic species, i.e., copper nitrates (15). As a consequence of the quite low pH of the impregnating solution some dissolution of the support is expected; through calcination both unsupported CuO and a disordered, amorphous surface layer, containing copper, titanium, oxygen, and nitrogen, will be produced. A phase, retaining some nitrogen, has already been observed in Cu/SiO_2 samples prepared by wet impregnation (16). The opposite situation is operating when preparing the catalyst by the C method. In this case the pH is 9, well above the zero charge point; thus the TiO_2 surface is negatively charged, favoring the adsorption of copper cations, while nitrate ions are removed by washing. In this case the ionic exchange reaction can account for the high dispersion observed on C samples.

A deeper understanding of the differences in the surface structure and composition of the two samples is obtained from the FTIR CO absorption analysis which will be presented in Section 3.3.

3.2. TPR Results

The samples prepared by incipient wetness technique (samples I, Fig. 3A, curves 1–3) show TPR patterns characterized by a narrow peak at 430 K, whose intensity appears to be independent of the copper loading, and a broader and stronger peak centered at 485 K and with a base width of about 90 K. The intensity of the latter peak rises with the copper loading, and meanwhile the copper specific surface area lowers (Table 1).

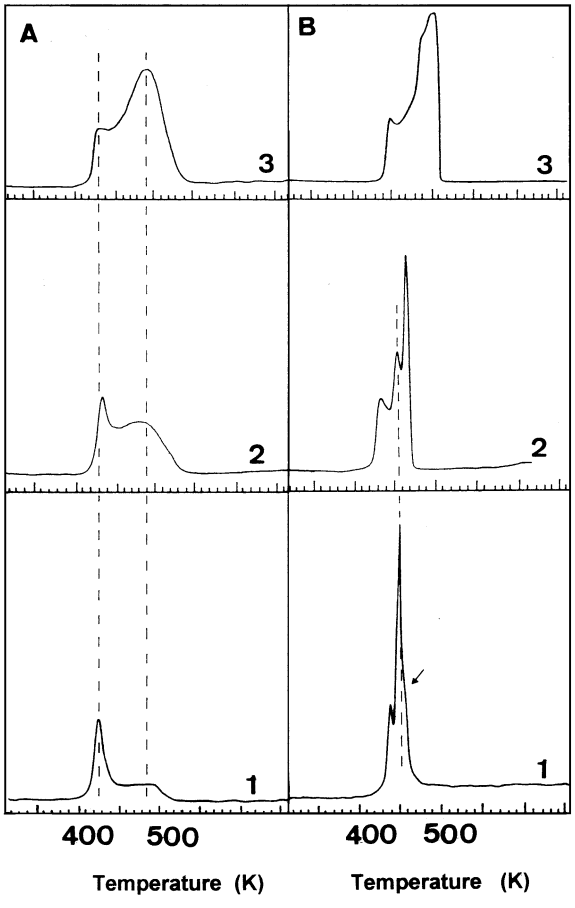

FIG. 3. TPR profiles of the calcined samples. (A): I samples: 1, 2I; 2, 4I; 3, 8I. (B): C samples: 1, 2C; 2, 4C; 3, 8C.

The samples prepared by the chemisorption-hydrolysis method (samples C, Fig. 3B, curves 1–3) show a small peak at 430 K, similar as regards intensity and position to that observed on samples I. However, instead of the one other broad peak detected in the I samples, at least two narrow peaks are present; these peaks for the more dilute samples are centered at 450 K, with a total base width of about 30 K. The copper surface area of these samples in much larger than with I samples (Table 1).

The broad reduction peak on I samples, centered at 485 K, can be ascribed mainly to the reduction of CuO particles having little or no interaction with the support. Looking to the increase of this peak with copper loading, this assignment appears in agreement with literature data concerning TPR profiles of bulk CuO derived from copper nitrate and from gerhardtite (17, 10). However, in the same temperature range there could also occur the reduction of the amorphous surface phase, formed by copper ions coordinated to oxygen atoms of titania, partially dissolved at the surface during the wet impregnation. This phase is highly dispersed and, by reduction, can generate isolated copper atoms, keeping a partial positive charge. An analogous situation has been observed on SiO_2-impregnated copper catalysts, where only one reduction peak is observed, although two copper-containing phases, a tenorite and a silicate-like one, are generally recognized.

On the contrary, CuO on C samples comes from chemisorption and slow hydrolysis of the cuprammine complex $[Cu(NH_3)_4]^{2+}$. TPR show that this species is very easily reduced, particularly at low copper loading. This feature, together with the high surface area and the absence of large crystallites in the precursor, suggests that the chemisorption–hydrolysis method leads to well-crystallized, very small copper oxide particles, easily reduced to metallic copper.

3.3. FTIR Characterization by CO Adsorption

Figures 4a and 4b show the IR absorbance at full coverage ($p = 10$ mbar) on the two differently prepared 4% samples, prereduced at different temperatures. On sample 4I423 (Fig. 4a, curve 1) the interaction with CO produces a very strong and broad band at 2113 cm^{-1}, integrated intensity (I) = 63 cm^{-1}, almost completely irreversible to the outgassing; on sample 4I523 (Fig. 4a, curve 2), a significantly weaker band at 2126 cm^{-1}, $I = 11$ cm^{-1}, and two weak bands at 2186 and 2208 cm^{-1} are observed; on the 4I673 sample (Fig. 4a, curve 3) a shift up to 2131 cm^{-1} and a decrease of the band intensity ($I = 2.1$ cm^{-1}) are observed. The bands at 2186 and at 2208 cm^{-1} are depleted by reduction of CO pressure; on the basis of their frequency and of their behavior, in agreement with literature data (19), they can be assigned to CO adsorbed on two different kinds of Ti^{4+} sites, i.e., the first one to titanium ions exposed on terraces, the second one to less coordinated step sites. The 2113–2131 cm^{-1} band is not affected by reduction of CO equilibrium pressure, but its intensity is significantly reduced after outgassing for increasing times, after 1 h the band being almost completely destroyed (not shown for sake of brevity).

On sample 4C423 a strong absorption band at 2110 cm^{-1} is produced by CO interaction (Fig. 4b, curve 1), showing a resistance to the outgassing similar to that of the sample I, pretreated in the same way; on sample 4C523 (Fig. 4b, curve 2) the CO interactions produces three bands, one at 2126 cm^{-1}, another at 2103 cm^{-1}, and a third at 2071 cm^{-1}. Moreover, a band at 2186 cm^{-1} is also observed. On sample 4C673 (Fig. 4b, curve 3) a narrow and quite strong band at 2129 cm^{-1} is produced by CO contact, while a quite weak and broad absorption at 2090 cm^{-1} and the two bands at 2186 and 2208 cm^{-1} are also observed. All the bands in the frequency 2131–2070 cm^{-1} range can be assigned to CO adsorbed on different copper sites. As the position of these bands in changing with the sample pretreatment, the copper loading, and the CO coverage, etc., for the sake of clarity in the following we will indicate as band I the band in the range 2123–2131 cm^{-1}, as band II the band in the range 2102–2118 cm^{-1}, and as band III the band in the range 2070–2090 cm^{-1}.

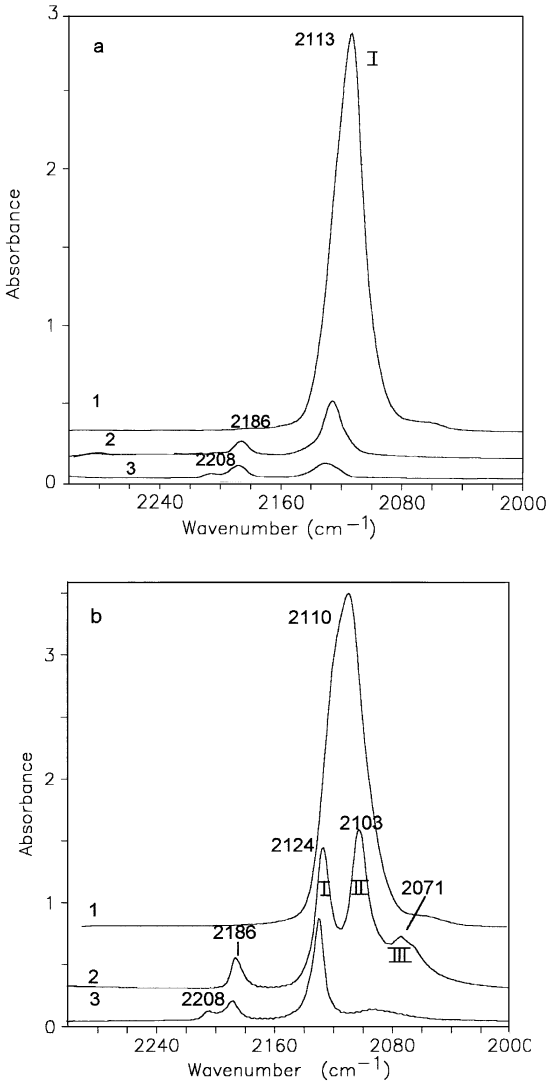

FIG. 4. IR absorption spectra of the carbonyl stretching region, taken after 10 mbar CO interaction on different samples. (a) 1, 4I423; 2, 4I523; 3, 4I673. (b) 1, 4C423; 2, 4C523; 3, 4C673.

In order to make a more precise assignment of these components we will examine their behavior with the CO coverage, copper loading, and sample pretreatment.

Bands II and III gradually reduce their intensity with the reduction of the CO equilibrium pressure and are completely removed simply by a short outgassing at RT, whereas band I is almost completely irreversible to the outgassing at RT (Fig. 5a, curves 1–6). By reporting for the sample 4C523 the integrated intensities of the three bands, obtained by curvefits of the experimental data of Fig. 5a with three Lorentzian bands, versus the frequency of their maxima (Fig. 5b), it is evident that band II shows a minimal frequency shift, by decreasing the coverage, from 2102 to 2106 cm^{-1}, while band III shows a larger shift, from 2071 to 2085 cm^{-1}. The frequency of band II; its half-width, 14 cm^{-1}; the strong dependence of its intensity on the equilibrium pressure; and the almost complete absence of the effect of the coverage on the frequency allow the assignment of this band to the adsorption of CO on Cu^0 step-edge sites. CO adsorption on copper single crystals has been extensively studied and similar frequencies were observed on stepped surfaces (20). It is worth noting that the bands observed on sample C are narrower than those observed on sample I or on many other supported copper catalysts reported in the literature (21) and they are quite similar to those observed on monocrystalline samples or on model samples (22). These findings appear to be an indication that C samples expose quite homogeneous and well-defined surface sites, at the surface of uniformly dispersed metal particles.

Band III is in the frequency range characteristic for CO chemisorbed on Cu^0 low-index planes; Cu(111) surface shows at low coverages a CO band at 2080 cm^{-1}, shifting to 2070 cm^{-1} at high coverages. CO adsorbed at the border of small copper particles can also contribute to this absorption. Similar features were also observed and discussed by Xu and Goodman (22) on model copper/SiO_2 samples, prepared by evaporating copper onto a planar silica thin film supported on Mo(110). Scanning tunneling microscopy (STM) of the same films showed different kinds of three-dimensional copper clusters with different surface structures, consistent with IRAS data (23). At very low copper coverages (<0.5 monolayer) an IR absorption band at 2062 cm^{-1} was observed by Xu and Goodman and was attributed to a particle size effect.

Similar features are observed also on sample 8C523 (Figs. 6a and b) and on sample 2C423 (Figs. 7a and b); however, some differences are noticed. On the first sample, with a higher loading in Cu, the intensities of the three absorptions assigned to CO adsorbed on copper sites have different relative strength: band II is significantly stronger, band I is weaker, the third component appears as a shoulder on the main absorption band, and the two bands at 2186 and 2208 cm^{-1} are completely absent. Moreover, band III shows a shift into a slightly different range, from 2078 to 2088 cm^{-1}, more similar to that observed on monocrystal(100) planes (20). On sample 2C423, characterized by a lower copper loading and by a lower reduction temperature, the main features observed are a larger blue shift by decreasing the CO coverage for band II, shifting from 2102 cm^{-1} up to 2118 cm^{-1}, and an abrupt change in band III at low coverages, shifting up to 2105 cm^{-1} (Figs. 7a and 7b). The more evident frequency shifts of the bands on this sample are probably related to the fact that in this sample, as a consequence of the low metal loading, the metal particles are very small, the dipole–dipole coupling interaction effects are reduced and the chemical shift effect is more evident. On this sample a smaller size of the metal particles, deduced from the IR spectra analysis, is also in agreement with the lower

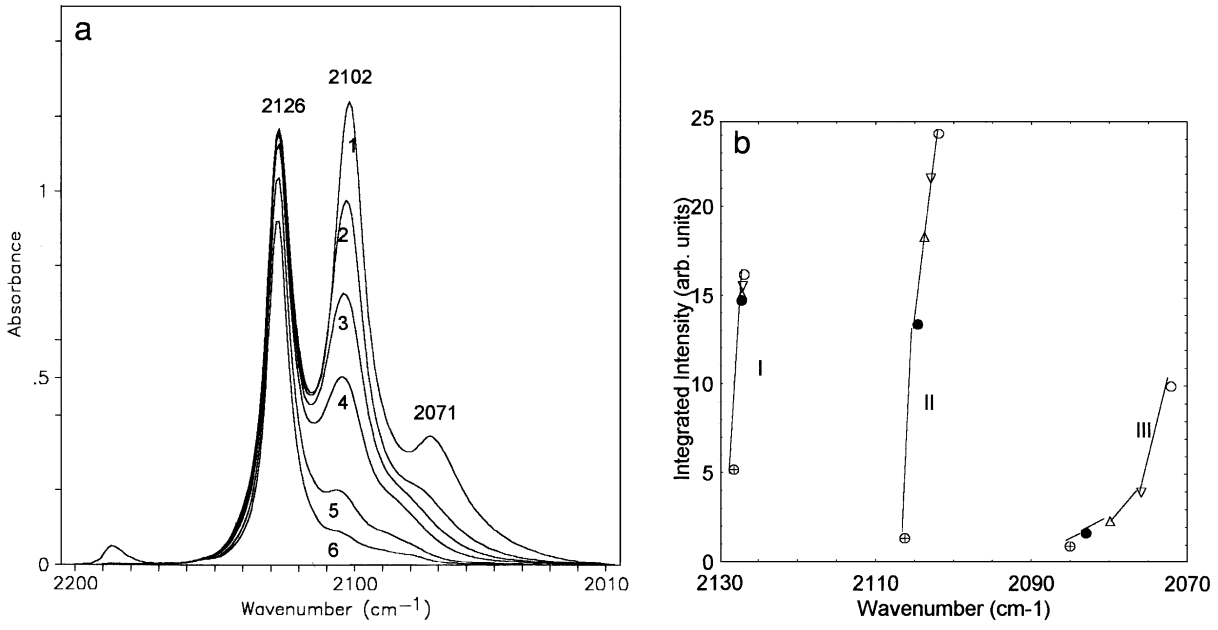

FIG. 5. (a) IR absorption spectra of CO adsorbed on sample 4C523: 1, 10 mbar CO; 2, 2 mbar; 3, 0.02 mbar; 4, 0.007 mbar; 5, 5 min evacuation; 6, 15 min evacuation. (b) Integrated intensities vs maximum frequencies of the bands obtained by fitting the curves of (a) with three Lorentzian bands.

reduction temperature of this sample, observed in the TPR experiments.

The evidence of an absorption band related to CO adsorbed on Cu(100) sites on the 8C523 sample can be an indication that by increasing the copper loading an increase in the metal particle size occurs. In fact, it can be shown that in a very small metal particle containing only 32 atoms, the number of corner, edge, (100) face, and (111) face atoms is 24, 0, 0, and 8, respectively, while in larger particles, as with an example containing more than 1000 atoms, also (100) sites are exposed (24). It can also be observed that on the 2C sample at low coverage the residual bands are at frequencies almost coincident with those reported by Moskovits and Hulse of the matrix isolated $COCu_n$ clusters, with $n = 2$, 3,

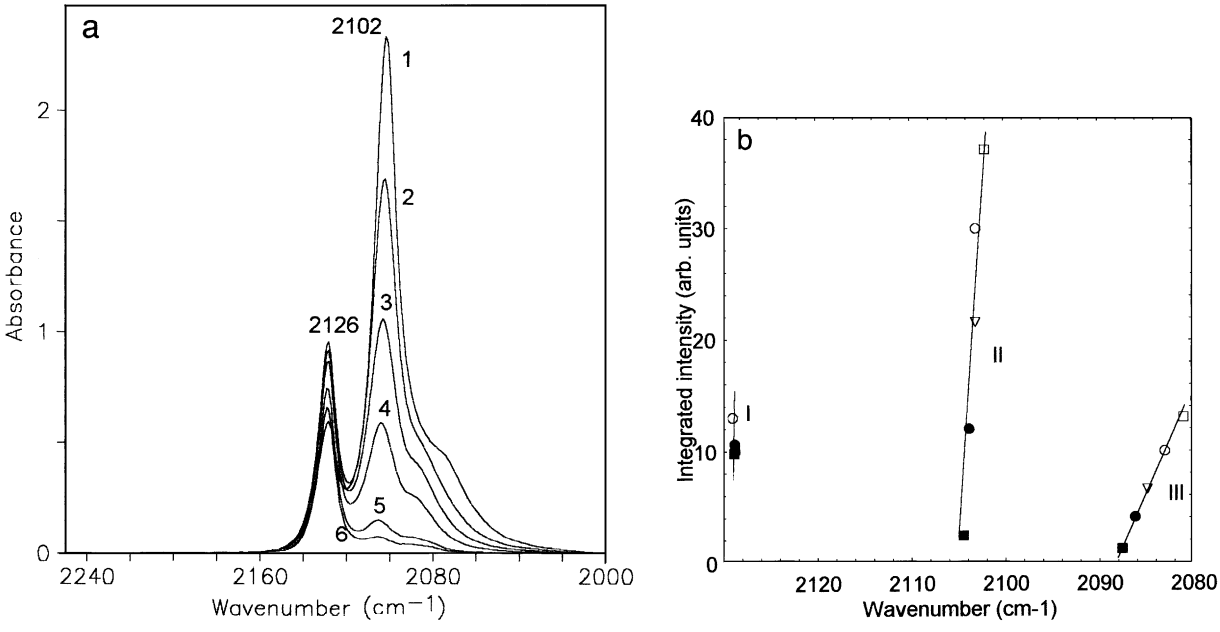

FIG. 6. (a) IR absorption spectra of CO adsorbed on sample 8C523: 1, 10 mbar CO; 2, 2 mbar; 3, 0.02 mbar; 4, 0.007 mbar; 5, 5 min evacuation; 6, 15 min evacuation. (b) Integrated intensities vs maximum frequencies of the bands obtained by fitting the curves of (a) with three Lorentzian bands.

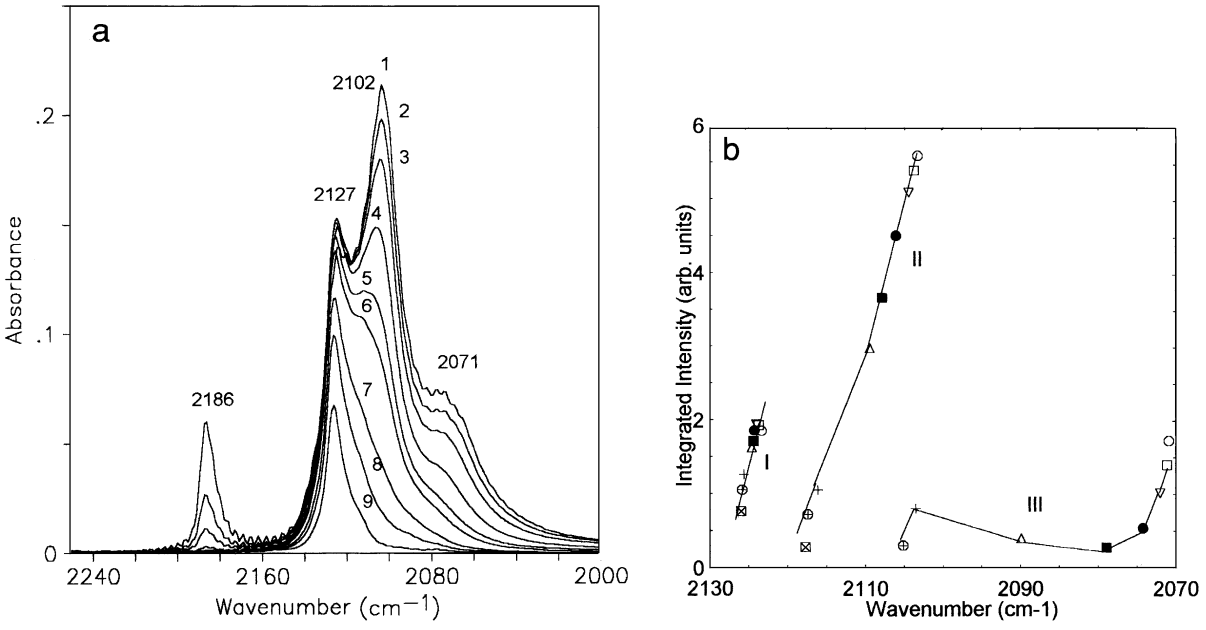

FIG. 7. (a) IR absorption spectra of CO adsorbed on sample 2C523: 1, 10 mbar CO; 2, 6 mbar; 3, 2 mbar; 4, 0.5 mbar; 5, 0.1 mbar; 6, 0.05 mbar; 7, 0.006 mbar; 8, 30 sec evacuation; 9, 5 min evacuation. (b) Integrated intensities vs maximum frequencies of the bands obtained by fitting the curves of section (a) with three Lorentzian bands.

and 4, respectively, namely at 2126, 2118 and 2105 cm^{-1} (25). The considerations on the morphology and metal particle dimensions of C samples made here from IR spectra analysis appear to be qualitatively in agreement with the specific Cu(0) area measurements reported in Table 1, where a decrease in the metallic area is observed on the sample with the higher metal loading.

As regards band I, even though the higher resistance to outgassing could suggest that the chemisorption sites might be copper ones in a more oxidized state, we prefer to assign this band to CO adsorbed on Cu^0 isolated sites. In fact, the band is present on C samples, with a higher intensity, after the most severe reductive treatments, up to 673 K (Fig. 4b, curve 3); it is also the only one observed, after reduction at 673 K on I sample (Fig. 4a, curve 3) and on 2C samples reduced at temperatures higher than 523 K (Fig. 7). A band at the same frequency was observed also on a sample previously studied, namely an amorphous alloy of Cu and Ti (26). A similar band was observed by Balkenende *et al.* (27) on Cu/SiO_2 samples prepared by homogeneous deposition of copper ions and reduced at 573–773 K. Based on the wavenumbers observed for Cu_nCO complexes (n ranging from 1 to 4) (25) the bands were ascribed to CO adsorption on coordinatively unsaturated or protruding Cu atoms. Goodman *et al.* (28, 29) observed similar features on well-characterized ultra-thin Cu films on Rh(100), Cu/Pt(111), and CuPt(111) surfaces: on these samples, together with the IR stretching frequency of adsorbed CO, the shifts in the XPS surface core binding energy produced by the substrates, the CO induced shift of the Cu($2p_{3/2}$) binding energy, and the shifts in the CO desorption temperature were determined. On these samples it was observed that C–O stretching frequency does not correlate with the amount of π-backdonation, as measured by the CO-induced shift of the Cu($2p_{3/2}$) binding energy. Therefore simple molecular orbital models do not allow a complete understanding of these features. The IR bands were also in these cases interpreted as arising from CO adsorption on isolated Cu atoms and/or on small two-dimensional Cu clusters, the frequency shift being interpreted as due to polarization interaction between the CO dipole and the charge density on the metal center. Recent theoretical calculations for CO adsorbed on Cu clusters indicate that polarization and charge transfer are the two main contributing factors to the Cu–CO bond and the magnitude of their relative contributions determine the bond strength, the charge polarization of Cu electron density away from the CO and the stretching frequency of the adsorbed CO (30). Similar polarization and charge transfer effects occur also when atoms and/or two-dimensional Cu small clusters are deposited at the surface of an oxidic support. UPS and EELS studies of ultra-thin copper films on TiO_2 evidenced a "positivization" of the copper atoms (31). This positivization might be associated with the interaction of the copper atoms with surface defects, such as V_0^+ and V_0^{2+} oxygen vacancies. It can be considered that very small clusters probably do not preserve their metallic properties; therefore their interaction with the oxidic support may no longer be governed by Schottky junction effects and they can be positivized by the interaction with the oxidic surface, in spite of the fact that the

interaction of *n*-type semiconductors with metal particles characterized by work functions higher than that of the support implies an electron transfer from the support to the metal. In fact, considering the electron affinity of titania and the work function of copper, a flow of electrons from the *n*-type semiconductor to the metal particles is expected: a thin sheet of *negative charge*, strongly localized at the interface between the metal and the oxide, is predicted in this case. However, the electrons will be strongly localized at the interface between the metal and the oxide; therefore, if the metal particles are thick enough, the charge transfer will not influence the surface chemical properties.

The complete absence of bands II and III on all the examined samples I can be taken as an indication that the impregnation method leads to samples in which three-dimensional copper metallic particles are lacking. This interpretation is in agreement with the HRTEM findings shown in Figs. 1 and 2, which indicate in the calcined C samples well-dispersed and crystalline particles and in the I samples an amorphous layer covering the titania microcrystals.

On increasing the reduction temperature of the 2C sample from 423 K (Fig. 8, curve 1) to 523 K (Fig. 8, curve 2) a significant increase in the high-frequency IR component is produced, and at the same time the 2102 and 2071 cm^{-1} components are almost completely destroyed: in this spectral region only a weak component at 2090 cm^{-1} is observed (Fig. 8, curve 2). A further increase in the reduction temperature up to 673 K produces an overall decrease of the CO absorption bands that appear, at the end of this treatment broader and more structured than before (Fig. 8, curve 3);

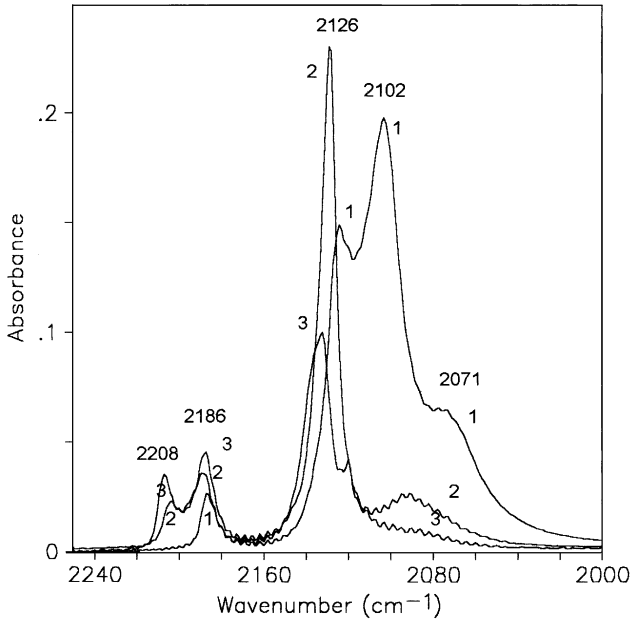

FIG. 8. IR absorption spectra of CO adsorbed on samples 2C differently pretreated: 1, 2C423: 2, 2C523; 3, 2C673.

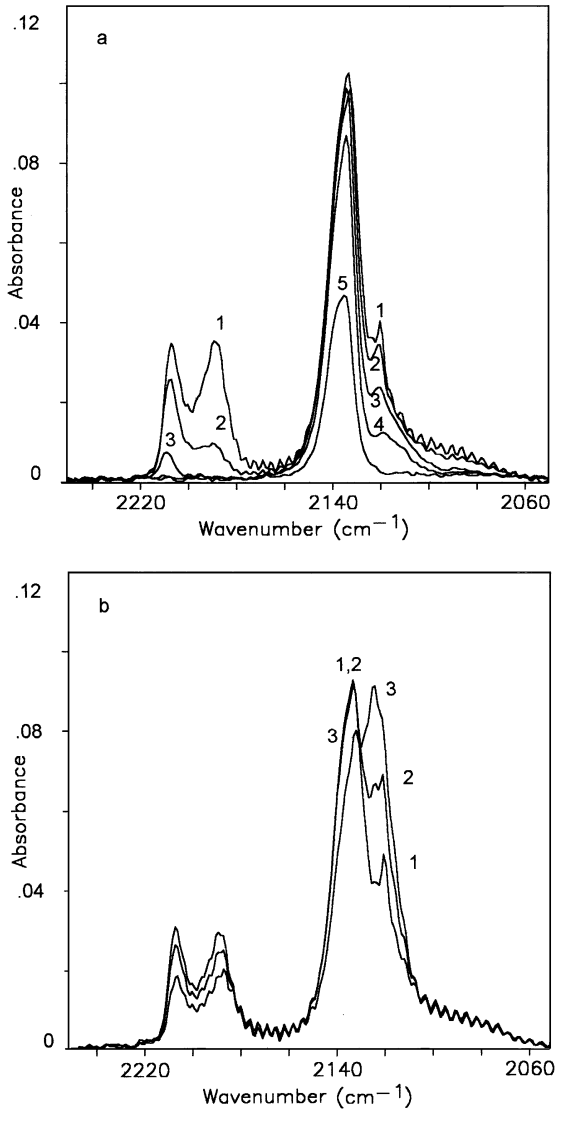

FIG. 9. IR absorption spectra of CO adsorbed on sample 2C673. (a) 1, 5 mbar; 2, 0.5 mbar; 3, 0.1 mbar; 4, 0.01 mbar; 5, 0.005 mbar. (b) Second interaction with 10 mbar of CO after different contact times: 1, 5 min; 2, 6 h; 3, 20 h.

two main components are identified, one at $\nu = 2134\ cm^{-1}$, slightly asymmetric, and another at 2120 cm^{-1}. A second CO adsorption after a new reduction at 673 K on the same sample produces the spectral features reported in Fig. 9b. This behavior can be interpreted as a rearrangement of adsorbed CO on similar copper sites exposed at the surface of small clusters of different nuclearity. The IR spectra of thin films of copper deposited on Rh and Pt (28, 29) showed different peaks at these frequencies which were assigned to copper clusters of different nuclearity. By reducing the CO pressure the 2186 and the 2208 cm^{-1} bands are quickly depleted; the 2120 cm^{-1} one is significantly reduced in intensity, while the 2134 cm^{-1} is only slightly modified (Fig. 9a).

The differences observed between the two experiments can be taken as an indication that the distribution of particle facets and clusters show some variability. In conclusion, on the C sample with the lowest copper loading, the spectroscopic features observed are quite similar to those of all the I samples examined; i.e., only isolated or small copper clusters are evidenced by CO chemisorption.

The almost completely isolated nature of the copper sites producing the absorption band at 2120–2130 cm^{-1} is clearly shown by the features observed in the spectra of ^{12}CO–^{13}CO 1 : 1 mixtures adsorbed on 2I samples reduced 673 K: two absorption bands with almost the same intensity are observed, one at 2123 cm^{-1} and another at 2075 cm^{-1} (Fig. 10), related to the two different isotopic species adsorbed on copper surface sites. The very small intensity transfer from the low-frequency band to the high-frequency one at the maximum coverage and the lack of any frequency shift by decreasing the coverage are clear indications that no dipole–dipole coupling between the adsorbed CO is acting on this sample, confirming that the adsorption sites related to the absorption band at 2120–2130 cm^{-1} are almost completely isolated.

By increasing the reduction temperature a strong decrease in the overall absorbance of CO chemisorbed on copper sites and a shift toward high frequencies is observed on both I and C Cu/TiO_2 samples. This behavior is completely different from that found for other copper-based catalysts, such as Cu/SiO_2 samples (27), where by increasing the reduction temperature an increase in the CO absorption band and a shift toward low frequencies is observed.

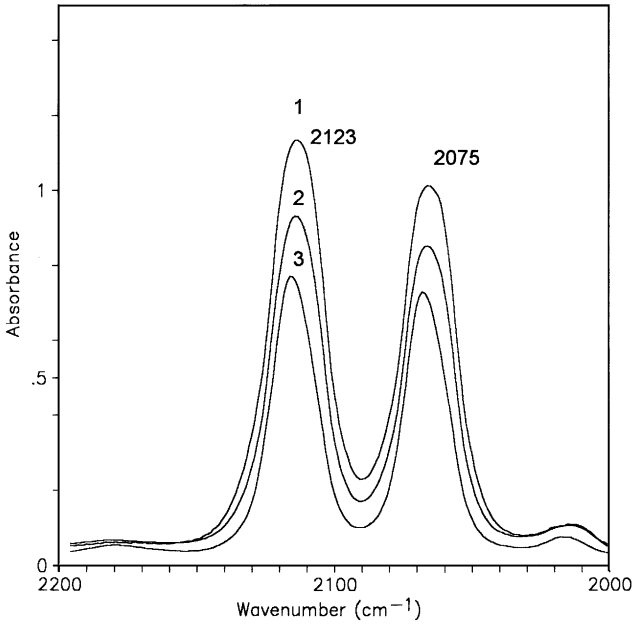

FIG. 10. IR absorption spectra of a ^{12}CO–^{13}CO mixture adsorbed on sample 2I673: 1, 10 mbar; 2, 2 mbar; 3, 0.05 mbar.

As already discussed before (26), in the case of copper supported on titania, by increasing the reduction temperature titania suboxides are formed, covering almost completely the copper particles and leaving at the surface isolated copper atoms. On the other hand, on silica-supported copper at low reduction temperature the reduction is not complete and thus the metal particles are rough, exposing copper clusters of different nuclearity and geometry, whereas by reduction at high temperatures, a coalescence of the small clusters occurs with the formation of flat extended Cu crystallites. The different surface chemical composition and its different evolution with the strength of the reductive treatments could be the reason for the different catalytic properties of copper supported on titania and on silica.

4. CONCLUDING REMARKS

The above data show quite clearly that samples with the same chemical composition can have very different properties, depending on the preparation method and on the thermal and chemical pretreatments.

The main differences revealed by the different characterization techniques employed are:

(i) HRTEM micrographs show a different behavior of the two calcined samples under the electron beam; on I samples the beam produces a large, amorphous layer covering the TiO_2 crystallites, while on C samples small particles are formed;

(ii) TPR profiles of C samples comprise narrow peaks in the range 450–500 K, while those of I samples are characterized by a broad peak at 440–530 K; the narrow peaks of C samples are assigned to the reduction of CuO crystallites of different dimensions, while the broad peak of I samples are assigned to both the reduction of unsupported CuO and to the reduction of a disordered phase containing copper and titania interdispersed at an atomic level, possibly with some residual anions;

(iii) the differences observed in the catalysts obtained by the two methods are probably related to the different pH of the solutions used in the preparation;

(iv) FTIR data provide evidence that the preparation method has a dramatic effect on the surface characteristics of the reduced catalysts: wet impregnation leads to a sample on which isolated or two-dimensional clusters of copper are exposed, whereas the chemisorption–hydrolysis method leads to three-dimensional copper particles;

(v) by increasing the copper loading on the C samples an increase in the metal particle dimensions can be inferred on the basis of both Cu(0) surface areas measured by N_2O decomposition and the CO adsorption IR data analysis;

(vi) increase in the reduction temperature decreases the number of exposed copper sites such that, at high reduction temperatures, both types of sample have sites which consist of almost completely isolated copper atoms; this

phenomenon is related to an almost complete coating of the Cu particles with reduced titania. In some respects, this behavior is similar to that usually observed for Group VIII noble metals supported on titania.

ACKNOWLEDGMENT

The financial support of Italian CNR, Progetto Finalizzato Chimica Fine Secondaria II, is acknowledged.

REFERENCES

1. Haller, G. L., and Resasco, D. E., *Adv. Catal.* **108**, 364 (1987) and references therein.
2. Wainwright, M. S., and Trimm, D. L., *Catal. Today* **23**, 29 (1995) and references therein.
3. (a) Okamoto, Y., Fukino, K., Imanaka, T., and Taranishi, S., *J. Phys. Chem.* **87**, 3737, 3747 (1983); (b) Sanchez, M. G., and Gazquez, J. L., *J. Catal.* **104**, 120 (1987).
4. Vong, M. S., Yates, M. A., Reyes, P., Perryman, A., and Sermon, P. A., *in* "Proceedings, 9th International Congress on Catalysis Calgary, 1988" (M. J. Phillips and M. Ternan, Eds.), Vol. 2, p. 545. Chem. Institute of Canada, Ottawa.
5. Delk, F. S. II, and Vanvere, A., *J. Catal.* **85**, 380 (1984).
6. Di Castro, V., Gargano, M., Ravasio, N., and Rossi, M., *in* "Preparation of Catalysts V" (G. Poncelet, P. A. Jacobs, and B. Delmon, Eds.), p. 95. Elsevier, Amsterdam, 1991.
7. Boccuzzi, F., Chiorino, A., Gargano, M., and Ravasio, N., *J. Catal.* **165**, 140 (1997).
8. Monti, D. A. M., and Baiker, A., *J. Catal.* **83**, 323 (1983).
9. Malet, P., and Caballero, A., *J. Chem. Soc. Faraday Trans. 1* **84**, 2369 (1988).
10. Fierro, G., Lo Jacono, M., Inversi, M., Porta, P., Lavecchia, R., and Cioci, F., *J. Catal.* **148**, 709 (1994).
11. Scholten, J. J. F., and Konvalinka, J. A., *Trans. Faraday Soc.* **65**, 2456 (1969).
12. Osinga, Th. J., Linsen, B. G., and van Beek, W. P., *J. Catal.* **7**, 277 (1967).
13. JCPDS 15-14 file, Oswald, H. R., *Z. Kristallogr.* **116**, 210 (1961).
14. Mc Cartney, M. R., and Smith, D. J., *Surf. Sci.* **221**, 214 (1989).
15. Brunelle, J. P., *Pure Appl. Chem.* **50**, 1211 (1978).
16. Higgs, V., and Pritchard, J., *Appl. Catal.* **25**, 149 (1986).
17. van der Grift, C. J. G., Mulder, A., and Geus, J. W., *Appl. Catal.* **60**, 181 (1990).
18. Boccuzzi, F., Guglielminotti, E., Martra, G., and Cerrato, G., *J. Catal.* **146**, 449 (1994).
19. Morterra, C., *J. Chem. Soc. Faraday I* **84**, 1617 (1988).
20. (a) Pritchard, J., Catterick, T., R. A., and Gupta, R. A., *Surf. Sci.* **53**, 1 (1975); (b) Hollins, P., and Pritchard, J., *Surf. Sci.* **89**, 486 (1979).
21. De Jong, K. P., Geus, J. W., and Joziasse, J., *Appl. Surf. Sci.* **6**, 273 (1980).
22. Xu, X., and Goodman, D. W., *J. Phys. Chem.* **97**, 683 (1993).
23. Xu, X., Vesecky, S. M., and Goodman, D. W., *Science* **258**, 788 (1992).
24. Brandt, R. K., Hughes, M. R., Bourget, L. P., Truszkowska, K., and Greenler, G. R., *Surf. Sci.* **286**, 15 (1993).
25. Moskovits, M., and Hulse, J. E., *Surf. Sci.* **61**, 302 (1976).
26. Boccuzzi, F., Baricco, M., and Guglielminotti, E., *Appl. Surf. Sci.* **70/71**, 147 (1993).
27. Balkenende, A. R., van der Grift, C. J. G., Meulenkamp, E. A., and Geus, J. W., *Appl. Surf. Sci.* **68**, 161 (1993).
28. Rodriguez, J. A., Campbell, R. A., and Goodman, D. W., *J. Phys. Chem.* **94**, 6936 (1990).
29. He, J. W., Kuhn, W. K., Leung, W. H., and Goodman, D. W., *J. Chem. Phys.* **93**, 7463 (1990).
30. Karl, B. E., Smith, R. J., and Berlowitz, P. J., *Surf. Sci.* **231**, 325 (1990).
31. Wu, M. C., and Moeller, P. J., *Surf. Sci.* **224**, 250 (1989).